Trampolinelike pulsating soliton fiber lasers

Yueqing Du, Chao Zeng, Zhiwen He, Qun Gao, Dong Mao,* and Jianlin Zhao

Key Laboratory of Light Field Manipulation and Information Acquisition, Ministry of Industry and Information Technology, MOE Key Laboratory of Material Physics and Chemistry under Extraordinary Conditions, Shaanxi Key Laboratory of Optical Information Technology, School of Physical Science and Technology, Northwestern Polytechnical University, NWPU, Xi'an 710129, China

(Received 23 May 2021; accepted 20 July 2021; published 3 August 2021)

Apart from stationary solitons originating from wave self-organization in ultrafast lasers, pulsating solitons have attracted lots of research interest due to their fantastic evolutionary behaviors, whose mechanisms are commonly dominated by dissipative effects such as gain, loss, and spectral filtering. Here, we demonstrate the trampolinelike pulsating soliton in the laser resonator originating from the conservative effects, i.e., Kerr effect and dispersion. It is found that the overdriven self-phase modulation induces the peak-to-dip transformation in the spectral domain, which is terminated by nonlinear spectral focusing due to the interplay between cross-phase modulation and anomalous dispersion. Such dynamic competition between the spectral broadening and focusing leads to the quasiperiodic peak-dip alternation with roundtrips like the trampoline game. A slow pulsation coexists with the trampolinelike fast pulsation due to the long-term soliton shaping. The simulation validates well experimental observations, fully revealing the underlying mechanism of the trampolinelike pulsating soliton. Having the potential to control laser stability, our results also show that the interplay between the Kerr effect and anomalous dispersion within laser cavities can trigger diverse transient phenomena in addition to the well-studied conventional soliton and modulation instability.

DOI: 10.1103/PhysRevA.104.023503

I. INTRODUCTION

Due to the nonconservative property of ultrafast fiber lasers, the dissipative soliton circulating inside the cavity exhibits many nontrivial transient behaviors [1,2]. With the recent progress of real-time spectroscopy such as the dispersive Fourier transform (DFT) technique [3], exploring transient and extreme dynamics in ultrafast lasers becomes a promising research topic [4–6]. The conventional soliton (CS) [7], stretched pulse [8], dissipative soliton [9], and similariton [10] correspond to fixed points in the phase space of the dissipative system, which have been in-depth investigated in nonlinear optics [7]. The fixed point transforms into a limit cycle through the Hopf bifurcation when adjusting the laser parameters, manifesting as a periodically pulsating soliton, also known as the breather [2,11–14].

Ascribed to the complex interaction of dissipation, dispersion, and nonlinearity, various pulsating solitons have been discovered in ultrafast lasers and Kerr cavities [15–19]. For example, the intensity and energy of soliton change periodically because of the dynamic balance between gain and loss [12]. The bandwidth breathing in the spectral domain arises from the competition between nonlinear spectral broadening and filtering [20]. Additionally, the soliton can pulsate by interacting with dispersive waves [15,21]. The spectral profile of the soliton changes dramatically from shot to shot periodically due to the composite filtering effect of the gain medium and fiber components [17,22,23] or energy redistribution induced by four-wave mixing (FWM) such as self-parametric amplification and parametric process [21,24,25].

Despite that diverse mechanisms of pulsating solitons have been proposed, the role of soliton-shaping dynamics in the form of the interplay between Kerr effect and anomalous dispersion is ignored in the context of pulsating solitons. The stationary pulses in anomalous-dispersion fiber lasers are shaped into the guide-center solitons in terms of the average properties along the cavity satisfying the fundamental soliton [26,27], whose self-consistency is disturbed by the overdriven nonlinearity. Previous simulations predict that the pulse splits and recovers chaotically arising from the high-order soliton properties, which is in the essence of the periodic competition between the Kerr effect and dispersion [28,29]. To date, the well-studied dynamics in nonlinear optical systems induced by the interplay between anomalous dispersion and Kerr effect are the CS and modulation instability. A question of theoretical value is whether the pulsating soliton in fiber lasers can be triggered by similar mechanisms within the conservative terms. More importantly, revealing the underlying mechanisms of a pulsating soliton helps to manipulate the performances of ultrafast fiber lasers for stability enhancement and dual-comb source.

In this paper, we report a type of pulsating soliton whose spectral center experiences the peak-dip alternation within several roundtrips (RTs). In analogy with the trampoline game, such a pulsating soliton is termed as the trampolinelike pulsating soliton (TLPS). Ascribed to the overdriven SPM, the spectrum splits into two peaks, i.e., the peak-to-dip transformation while the intrapulse cross-phase modulation (XPM) and the anomalous-dispersion force spectral peaks to merge.

*Corresponding author: maodong@nwpu.edu.cn

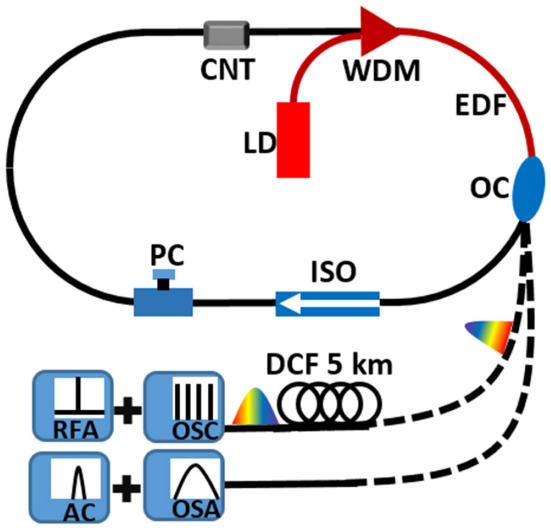

FIG. 1. Schematic configuration of the experimental setup. LD: laser diode, WDM: wavelength-division-multiplexer, EDF: erbium-doped fiber, OC: output coupler, ISO: isolator, PC: polarization controller, CNT: carbon nanotube, DCF: dispersion compensating fiber, OSC: oscilloscope, RFA: radio frequency analyzer, OSA: optical spectrum analyzer, AC: autocorrelator.

Additionally, the soliton-shaping-induced slow pulsation is accompanied by the fast pulsation.

Numerical simulations validate experimental observations, confirming that the pulsation with the peak-dip alternation is a phenomenon induced by the interplay between anomalous dispersion and Kerr effect. The underlying mechanism of the TLPS helps to explore complex wave dynamics in the spectral domain such as the spectral rogue waves and solitons [30–32].

II. EXPERIMENTAL RESULTS

The schematic configuration of the fiber laser is shown in Fig. 1, which comprises 0.8 m Er-doped fiber (EDF, Nufern) and 6.06 m single-mode fiber (SMF). The Kerr nonlinearity of the EDF and SMF is 1.69 and 1.3 W^{-1} km^{-1}, respectively. The pump light was injected into the EDF through a 980/1550 wavelength-division multiplexer. The unidirectional operation of the laser was ensured by a polarization-insensitive isolator. A single-wall carbon nanotube film was used as the mode locker, and the pulse was extracted from a 7:3 output coupler (OC). The DFT was realized via a 5 km dispersion compensating fiber (total dispersion of 750 ps/nm), a 5 GHz photoelectric detector, and a 4 GHz real-time oscilloscope.

The stationary mode-locking state appeared by setting the pump power at 25 mW and tuning the polarization controller (PC) [Figs. 2(a) and 2(b)]. The output spectrum displayed characteristic Kelly sidebands of solitons, by which the net dispersion of the cavity was calculated to be $-0.183\,ps^2$ (e.g., $-61.65\,ps^2/km$ for EDF and $-22\,ps^2/km$ for SMF). The signal-to-noise ratio of ∼60 dB without modulating sidebands on the radiofrequency (RF) spectra confirms the stable mode-locking state and agrees with the 6.86 m cavity length. The pulsating soliton was obtained by adjusting the PC until a spectral peak and additional subsidebands formed on the spectrum [Fig. 2(c)], whose pulsating property manifested as

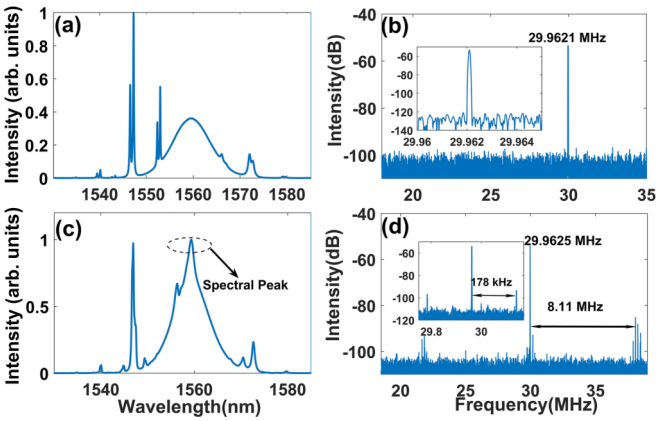

FIG. 2. Results of the stationary and pulsating mode-locking states. Stationary mode-locking at the pump power of 25 mW: (a) optical spectrum and (b) radiofrequency (RF) spectrum. Pulsating mode-locking at the pump power of 25 mW: (c) optical spectrum and (d) RF spectrum.

modulating sidebands on the RF spectrum [Fig. 2(d)]. One can note that there are two rhythms of the pulsation, i.e., the faster one is ∼8.11 MHz, while the slower one is ∼178 kHz (inset).

The real-time spectral evolution of the pulsating soliton is displayed in Fig. 3. The peak-dip alternation of spectral center over eight single-shot spectra [Fig. 3(a)] is analogous to the trampoline game; thereby, this unique state is named TLPS. The spectral profile of the TLPS changes from shot to shot with discontinuity [Figs. 3(a) and 3(b)], corresponding to the fast pulsation with the frequency of 8.11 MHz. In the context of a longer timescale, as shown in Fig. 3(c), the spectrum pulsates at a period of ∼167.8 RTs (5.6 μs and 178.6 kHz), in agreement with the slow pulsating frequency of 178 kHz on the RF spectrum [inset of Fig. 2(d)]. The average spectra over 4000 single shots [upper panel of Fig. 3(c)] fit well with that measured by the optical spectrum analyzer (OSA) [Fig. 2(c)], verifying the accuracy of the DFT measurement. Note that the narrow spectral peak on the spectrum by OSA [Fig. 2(c)] is reproduced by DFT [upper panel of Fig. 3(c)], indicating the coherence of this spectral peak is distinct from the quasicontinuous-wave spectral peak in the soliton rain mode locking [33].

As shown in the right panel of Fig. 3(c), the slow pulsation with 178.6 kHz manifests as six big envelopes over 1000 RTs, in which the oscillating fringes correspond to the fast pulsation of 8.11 MHz. For the spectrum of a nonlinear wave, the peak-to-dip transformation [from first to third RT in Fig. 3(a)], usually induced by the overdriven SPM, is ubiquitous in various fields of nonlinear optics. As shown in Fig. 3(a), a reverse process, i.e., the dip-to-peak transformation, is observed in the evolution to ensure the self-consistency (from third to fourth RT), whose mechanism is lacking in the literature. The dip-to-peak transformation is impossible to be induced by the reverse FWM, considering the all-anomalous-dispersion configuration of our laser [25]. In addition, we have checked that the TLPS with the peak-dip alternation can be observed with different laser parameters, indicating the generality of this nontrivial phenomenon. Thereby, the origination of this nontrivial TLPS needs to be further explored.

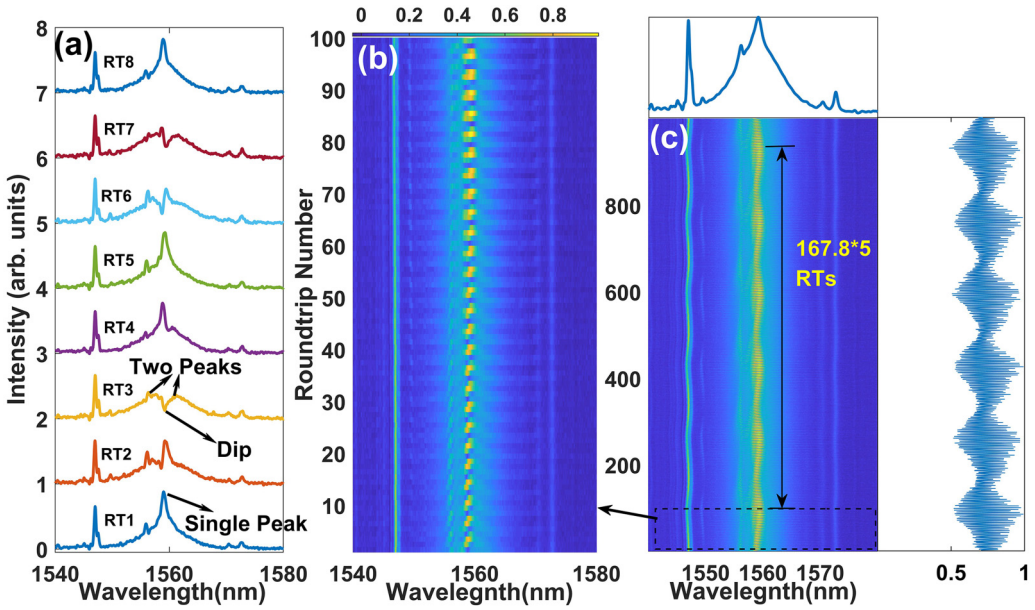

FIG. 3. Real-time spectral evolution captured by the dispersive Fourier transform (DFT) at the pump power of 25 mW. (a) Consecutive eight single-shot spectra. (b) Shot-to-shot evolution over 100 roundtrips (RTs). (c) Shot-to-shot evolution over 1000 RTs. Upper panel of Fig. 2(c): Average spectrum over 4000 RTs. The right panel of Fig. 2(c): Peak intensity evolution of the DFT signal.

III. SIMULATION RESULTS

We performed numerical simulations to reveal the underlying mechanism of TLPS. The coupled generalized nonlinear Schrödinger equations were used to model the pulse propagation and solved by the symmetric split-step Fourier method:

$$\frac{\partial u}{\partial z} = i\beta u - \delta\frac{\partial u}{\partial t} - i\frac{\beta_2}{2}\frac{\partial^2 u}{\partial t^2} + \beta_3\frac{\partial^3 u}{\partial t^3} + \frac{g}{2}u + i\gamma|u|^2 u + i\gamma\frac{2|v|^2}{3}u + \frac{i\gamma u^* v^2}{3} + \frac{g}{2\Omega_g^2}\frac{\partial^2 u}{\partial t^2}, \tag{1}$$

$$\frac{\partial v}{\partial z} = -i\beta v + \delta\frac{\partial v}{\partial t} - i\frac{\beta_2}{2}\frac{\partial^2 v}{\partial t^2} + \beta_3\frac{\partial^3 v}{\partial t^3} + \frac{g}{2}v + i\gamma|v|^2 v + i\gamma\frac{2|u|^2}{3}v + \frac{i\gamma v^* u^2}{3} + \frac{g}{2\Omega_g^2}\frac{\partial^2 v}{\partial t^2}, \tag{2}$$

$$g = g_0 \exp\left[-\frac{\int(|u|^2+|v|^2)dt}{E_s}\right], \tag{3}$$

$$T = 1 - loss - \frac{md}{1+\frac{P}{P_s}}. \tag{4}$$

The variables u and v are the complex amplitudes of the slow and fast components, respectively. Here, z and t correspond to the propagation distance with the unit of m and retard time, respectively. Also, $\beta = \pi/L_b$ and $\delta = \lambda/2cL_b$ relate to the linear birefringence of fiber with a beat length L_b. Furthermore, β_2, β_3, and γ are the group-velocity dispersion, third-order dispersion, and nonlinear coefficient of fiber, respectively. The gain bandwidth of the EDF (20 nm) is determined by Ω_g. Here, g_0 is the small-signal gain, while E_s represents the saturation energy of the EDF, and the value of g_0 is set to be zero in the SMF. The property of the SA depends on the nonsaturable loss ($loss$), modulation depth (md), and saturable power (P_s). Here, P is the instantaneous power of the soliton. The simulation parameters were set as follows to match those in the experiment: $L_b = 2\,\mathrm{m}$, $\beta_3 = 0.1\,\mathrm{ps}^3/\mathrm{km}$, $g_0 = 13\,\mathrm{m}^{-1}$, $loss = 0.55$, $md = 6.46\%$, and $P_s = 37\,\mathrm{W}$.

The shot-to-shot evolution of the TLPS at the saturation energy of 112 pJ is shown in Fig. 4, in which the spectral center pulsates with a trampolinelike behavior at a timescale of several RTs, agreeing with the fast pulsation in the experiment [Fig. 4(b)]. In the long-term evolution of 2000 RTs [Figs. 4(b) and 4(c)], a slow pulsation evolves with a period of ~371 RTs, which is the same order of magnitude as that of the experiment. As shown in Fig. 4(c), despite that the spectral intensity pulsates with a large amplitude, the normalized energy is confined in a small range (from 0.976 to 1), indicating a quasibalance between the gain and loss during evolution. Due to the soliton shaping of the TLPS that deviates from the fundamental soliton, the strong radiation of dispersive waves is always accompanied by the enhancement of the spectral center [Fig. 4(d)], which results in the slow pulsation. One can see the numerically simulated shot-to-shot evolution (Fig. 4) agrees with the experiment (Fig. 3), ensuring the suitability of the subsequent research on the intracavity dynamics of the PLTS, as illustrated in Fig. 5.

The spectra at the output port [Fig. 5(a)] in eight consecutive RTs agree qualitatively with the experimental results [Fig. 3(a)]. The TLPS experiences twice the peak-dip alternations in eight RTs during the intracavity propagation [Fig. 5(b)], leading to the exotic change of spectral profiles between adjacent RTs at the output port. The spectrum splits into two peaks along the cavity positions (e.g., 0–13 m), where the overdriven SPM-induced pulse distortion cannot be balanced by the dispersion, manifesting as the peak-to-dip transformation from RT1 to RT3. Two peaks gradually merge

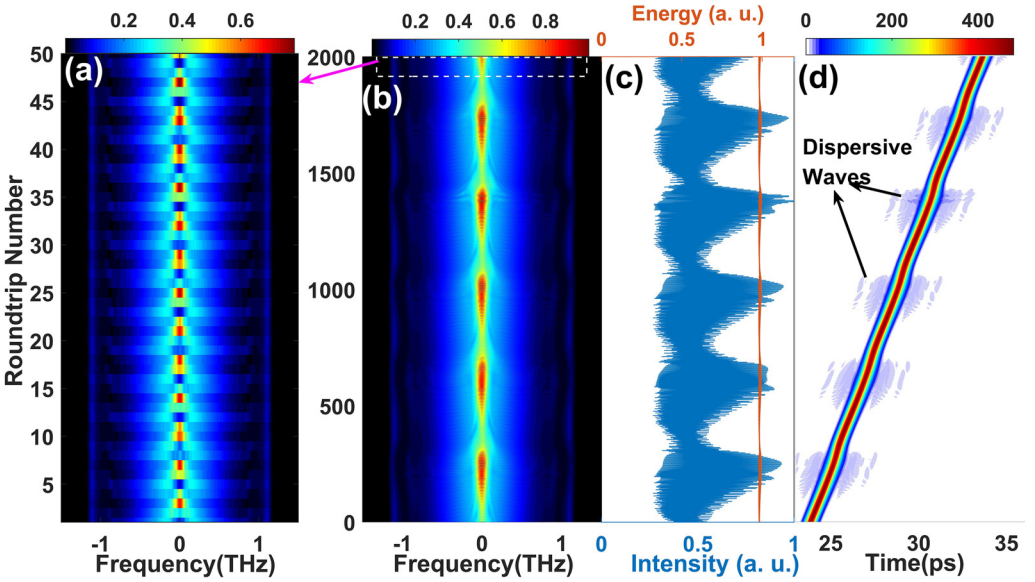

FIG. 4. Trampolinelike pulsating soliton at the saturation energy of 112 pJ. (a) Shot-to-shot evolution of the spectrum over 50 roundtrips (RTs). (b) Shot-to-shot evolution of the spectrum over 2000 RTs. (c) Normalized spectral intensity and energy evolutions over 2000 RTs. (d) Shot-to-shot evolution of the temporal pulse over 2000 RTs.

from 15 to 22 m in the cavity [Fig. 5(b)], i.e., the dip-to-peak transformation from RT3 to RT4, which is essential for realizing self-consistency of the TLPS. The joint time-frequency spectrograms of the slow-axis component of the TLPS at three marked cavity positions [Figs. 5(c)–5(e)] reveal the spectral focusing (dip-to-peak transformation) in the third RT. The soliton has two spectral peaks in Fig. 5(c) at the shorter and longer wavelength sides, which are marked by PB and PR, respectively. During propagating in the SMF, PB moves ahead of PR in the temporal domain because of the anomalous dispersion [Fig. 5(d)]. By viewing PB and PR as two independent parts, the Kerr effect can be divided into SPM, XPM, and FWM (between PB and PR). In the temporal domain, the PB tail induces XPM on the PR head, driving the PR spectrum toward the shorter wavelength side. Similarly, the PR head will drive that of PB to the longer wavelength side. As a result, PB and PR move toward the central wavelength, as displayed in Fig. 5(e), inducing the dip-to-peak transformation. Thus, we conclude that the intrapulse XPM together with the anomalous dispersion drives the dip-to-peak transformation, i.e., the nonlinear spectral focusing. In the context of real-time evolutions of lasers via DFT, our findings help to understand the wave dynamics in the spectral domain, such as spectral focus, wavelength shifting, and collisions between spectral

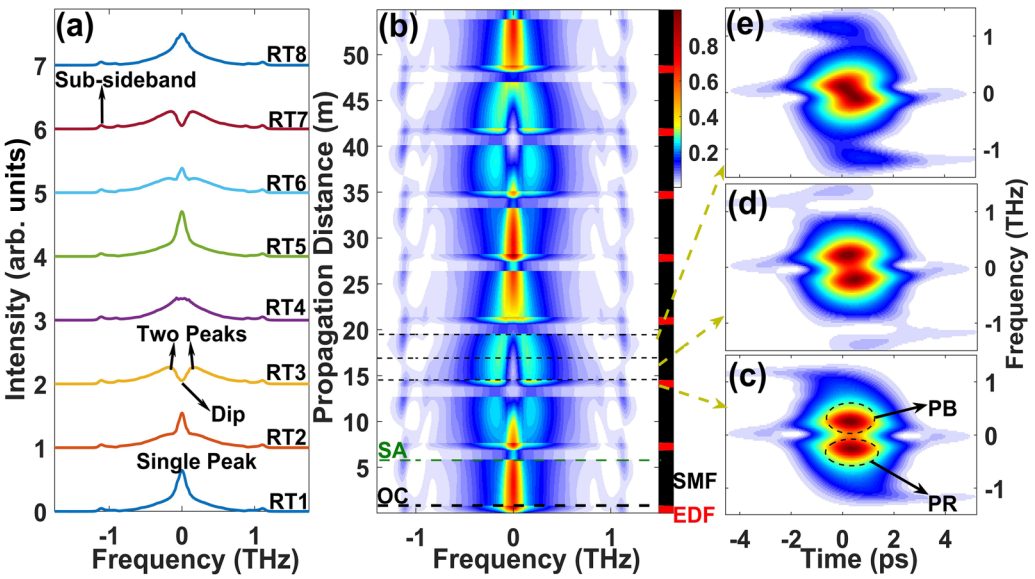

FIG. 5. Intracavity evolution of the fast pulsation at the saturation energy of 112 pJ. (a) Single-shot spectra of eight consecutive roundtrips (RTs). (b) Intracavity spectral evolution in eight consecutive RTs. (c)-(e) Time-frequency spectrograms of the slow-axis component at three cavity positions in the single-mode fiber (SMF).

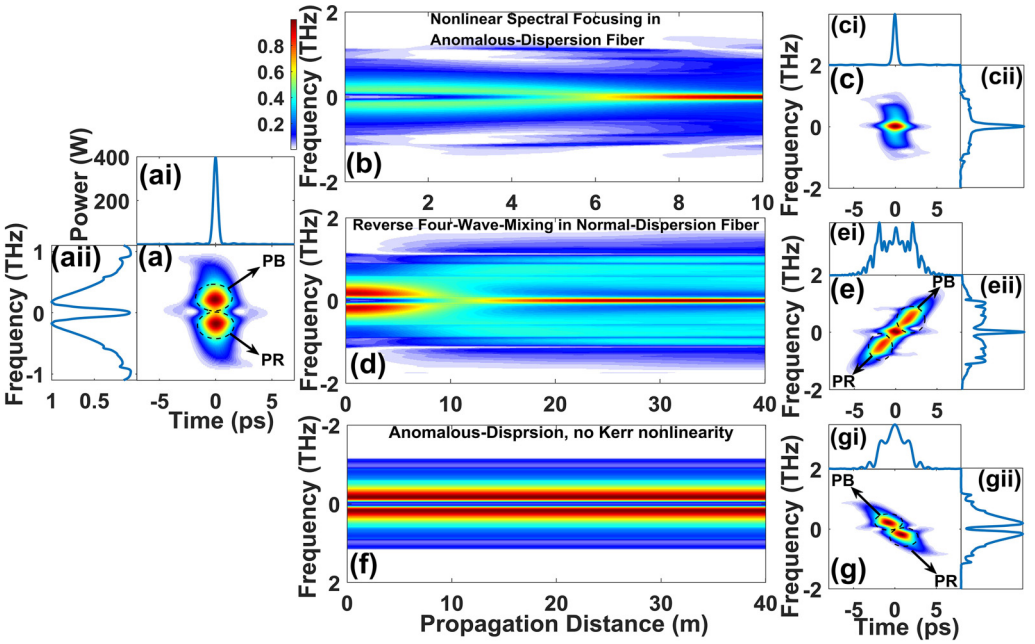

FIG. 6. Propagating properties of the soliton with two spectral peaks in different mediums. (a) Spectrogram of the soliton with two peaks: (ai) temporal profile and (aii) spectral profile. (b) Nonlinear spectral focusing in the 10-m single-mode fiber (SMF) with anomalous dispersion, ($-22\,\mathrm{ps}^2/\mathrm{km}$, $1.3\,\mathrm{W}^{-1}\,\mathrm{km}^{-1}$). (c) Spectrogram at the end of the fiber: (ci) spectral profile at the end of 10-m SMF and (cii) temporal profile at the end of 10-m SMF. (d) Reverse four-wave mixing in 40-m fiber with normal dispersion ($22\,\mathrm{ps}^2/\mathrm{km}$, $1.3\,\mathrm{W}^{-1}\,\mathrm{km}^{-1}$). (e) Spectrogram at the end of 40-m normal-dispersion fiber: (ei) temporal profile at the end of 40-m normal-dispersion fiber and (eii) spectral profile at the end of 40-m normal-dispersion fiber. (f) Linear propagation in anomalous-dispersion medium without Kerr nonlinearity ($-22\,\mathrm{ps}^2/\mathrm{km}$, $0\,\mathrm{W}^{-1}\,\mathrm{km}^{-1}$). (g) Spectrogram at the end of the 40-m linear dispersion medium: (gi) temporal profile at the end of the 40-m linear dispersion medium and (gii) spectral profile at the end of the 40-m linear dispersion medium.

peaks, which are significant to reveal the mechanism of the spectral rogue waves and solitons [30–32].

The mechanism of the nonlinear spectral focusing can be further confirmed by simulating its distinct propagating dynamics in different mediums (Fig. 6). The distorted soliton caused by the overdriven SPM has a smooth temporal profile [Fig. 6(ai)] and spectral profile with two peaks marked by PB and PR [Figs. 6(a) and 6(aii)]. After propagating in a 10 m SMF with anomalous dispersion, PB and PR attract each other until they absolutely merge in the spectral domain, i.e., the dip-to-peak transformation, which is clearly visualized in Figs. 6(b) and 6(c), validating the explanation of the nonlinear spectral focusing for the TLPS.

In the presence of normal dispersion, as shown in Fig. 6(d), the dip-to-peak transformation also happens due to the reverse FWM without merging of PB and PR [Fig. 6(e)]. As the PB is ahead of PR in the temporal domain, the soliton has a distorted temporal profile [Fig. 6(ei)] that is incompatible with the self-consistency for the TLPS in the cavity, which is different from the undistorted temporal profile under the nonlinear spectral focusing [Fig. 6(ci)]. Although the reverse FWM induces a spectral peak in Fig. 6(eii), PB and PR constitute the quasiflat pedestal, which is also a clear difference with the case under nonlinear spectral focusing [Fig. 6(cii)].

In the linear medium, the spectral profile is invariant during propagation [Figs. 6(f) and 6(gii)] with PB ahead of PR due to anomalous dispersion [Fig. 6(g)], resulting in the oscillating structures in the temporal domain [Fig. 6(gi)] due to the interference between PB and PR.

Two spectral peaks of the soliton can be regarded as a soliton molecule in the spectral domain, whose mutual attraction is induced by the SPM, while the repulsion originates from the interplay between XPM and anomalous dispersion. The competition between the repulsion and attraction gives rise to periodical collision inside the spectral soliton molecule, manifesting as the peak-dip alternation of the TLPS. Moreover, in contrast to the silent evolution in the temporal domain, the spectra of the TLPS have exotic evolutionary behaviors, inspiring us to further study the localized soliton, wave collisions, and rogue waves in the spectral domain.

IV. CONCLUSIONS

The TLPS in an anomalous-dispersion fiber laser is revealed through experiments and simulations. The spectral center of the TLPS continuously undergoes the peak-dip alternation, manifesting as the fast shot-to-shot pulsation, which arises from the dynamic interplay between the anomalous dispersion and overdriven Kerr effect. The overdriven SPM induces the peak-to-dip transformation of the spectrum, while the reverse process is much more complex: (i) the dispersion pulls the shorter wavelength peak ahead of the longer wavelength peak in the temporal domain, and (ii) the intrapulse XPM induces a mutual attraction between spectral peaks in the spectral domain, merging them into one peak, i.e., the dip-to-peak transformation. The slow pulsation of the TLPS is the result of the long-term soliton shaping accompanied by dispersive wave radiation. Apart from the specific TLPS

phenomenon disclosed in this paper, our results also show that the interplay between anomalous dispersion and Kerr effect can induce abundant nonlinear phenomena within laser cavities in addition to the well-known CS and modulation instability. The spectral brightness enhancement during the dip-to-peak transformation develops a possible mechanism of the spectral rogue wave and soliton in nonlinear optics. In addition, the joint time-frequency analysis is a powerful tool to research solitons with complex temporal and spectral evolutionary behaviors in fiber lasers.

ACKNOWLEDGMENTS

This paper was supported by the National Natural Science Foundation of China (No. 61805277, No. 11634010, and No. 11874300), the Natural Science Basic Research Program of Shaanxi (No. 2021JC-09, 2019JQ-447), the Fundamental Research Funds for the Central Universities (No. 310202011QD003, No. 3102019JC008, and No. 3102019PY002), and the National Key R&D Program of China (No. 2017YFA0303800).

[1] P. Grelu and N. Akhmediev, Nat. Photonics **6**, 84 (2012).
[2] J. M. Soto-Crespo, M. Grapinet, P. Grelu, and N. Akhmediev, Phys. Rev. E **70**, 066612 (2004).
[3] K. Goda and B. Jalali, Nat. Photonics **7**, 102 (2013).
[4] G. Herink, F. Kurtz, B. Jalali, D. R. Solli, and C. Ropers, Science **356**, 50 (2017).
[5] A. F. J. Runge, N. G. R. Broderick, and M. Erkintalo, Optica **2**, 36 (2015).
[6] K. Krupa, K. Nithyanandan, U. Andral, P. Tchofo-Dinda, and P. Grelu, Phys. Rev. Lett. **118**, 243901 (2017).
[7] V. J. Matsas, T. P. Newson, D. J. Richardson, and D. N. Payne, Electron. Lett. **28**, 1391 (1992).
[8] W. He, M. Pang, C. R. Menyuk, and P. St. J. Russell, Optica **3**, 1366 (2016).
[9] A. Chong, J. Buckley, W. Renninger, and F. Wise, Opt. Express **14**, 10095 (2006).
[10] F. O. Ilday, J. R. Buckley, W. G. Clark, and F. W. Wise, Phys. Rev. Lett. **92**, 213902 (2004).
[11] J. Peng, S. Boscolo, Z. Zhao, and H. Zeng, Sci. Adv. **5**, eaax1110 (2019).
[12] Y. Du, Z. Xu, and X. Shu, Opt. Lett. **43**, 3602 (2018).
[13] T. Xian, L. Zhan, W. Wang, and W. Zhang, Phys. Rev. Lett. **125**, 163901 (2020).
[14] A. E. Akosman and M. Y. Sander, Sci. Rep. **8**, 13385 (2018).
[15] Y. Du, M. Han, P. Cheng, and X. Shu, Opt. Lett. **44**, 4087 (2019).
[16] Z. Wang, Q. Jiang, Z. Tang, and Z. Zhang, Opt. Express **28**, 28209 (2020).
[17] J. Chen, X. Zhao, T. Li, J. Yang, J. Liu, and Z. Zheng, Opt. Express **28**, 14127 (2020).
[18] F. Leo, L. Gelens, P. Emplit, M. Haelterman, and S. Coen, Opt. Express **21**, 9180 (2013).
[19] E. Lucas, M. Karpov, H. Guo, M. Gorodetsky, and T. Kippenberg, Nat. Commun. **8**, 736 (2017).
[20] J. Peng and H. Zeng, Phys. Rev. Appl. **12**, 034052 (2019).
[21] M. Liu, Z.-W. Wei, H. Li, T.-J. Li, A.-P. Luo, W.-C. Xu, and Z.-C. Luo, Laser & Photon. Rev. **14**, 1900317 (2020).
[22] C. Bao, W. Chang, C. Yang, N. Akhmediev, and S. T. Cundiff, Phys. Rev. Lett. **115**, 253903 (2015).
[23] Z. Wen, K. Wang, H. Chen, B. Lu, and J. Bai, Opt. Express **28**, 28033 (2020).
[24] J. Peng and H. Zeng, Phys. Rev. Appl. **11**, 044068 (2019).
[25] S. K. Turitsyn, A. E. Bednyakova, M. P. Fedoruk, S. B. Papernyi, and W. R. L. Clements, Nat. Photonics **9**, 608 (2015).
[26] H. A. Haus, J. Appl. Phys. **46**, 3049 (1975).
[27] A. Hasegawa and Y. Kodama, Phys. Rev. Lett. **66**, 161 (1991).
[28] Y. Du, M. Han, and X. Shu, IEEE Photonics J. **12**, 1 (2020).
[29] G. P. Agrawal, *Nonlinear Fiber Optics*, 4th ed. (Springer, Berlin, Heidelberg, 2007).
[30] A. Picozzi, S. Potois, and G. Millot, Phys. Rev. Lett. **101**, 093901 (2008).
[31] W. Liu, S. Zhang, and W. Frank, Opt. Lett. **40**, 1366 (2015).
[32] Y. Zhou, Y. Ren, J. Shi, and K. Wong, Photon. Res. **8**, 1566 (2020).
[33] S. Chouli and P. Grelu, Opt. Express **17**, 11776 (2010).